POLITECNICO DI TORINO
Repository ISTITUZIONALE

Waste to life: Low-cost, self-standing, 2D carbon fiber green Li-ion battery anode made from end-of-life cotton textile

Terms of use:

(Article begins on next page)

19 April 2024

Waste to life: low-cost, self-standing, 2D carbon fiber green Li-ion battery anode made from end-of-life cotton textile

Pravin Jagdale[a,b,*], Jijeesh Ravi Nair[c,*], Aamer Khan[b], Marco Armandi[b], Giuseppina Meligrana[d,e], Francisco Robles Hernandez[f,g], Irene Rusakova[h], Erik Piatti[b], Massimo Rovere[b], Alberto Tagliaferro[b], Martin Winter[c,i,l], Claudio Gerbaldi[d,e*]

[a] Center for Sustainable Future Technologies, Italian Institute of Technology (IIT), Via Livorno 60, 10144, Torino, Italy.

[b] Department of Applied Science and Technology (DISAT), Politecnico di Torino, C.so Duca degli Abruzzi, 24, 10129, Torino, Italy.

[c] Institute of Energy and Climate Research (IEK-12), Forschungszentrum Jülich GmbH, Helmholtz Institute Münster, Corrensstraße 46, 48149 Münster, Germany.

[d] GAME Lab, Department of Applied Science and Technology (DISAT), Politecnico di Torino, C.so Duca degli Abruzzi, 24, 10129, Torino, Italy.

[e] National Reference Center for Electrochemical Energy Storage (GISEL) - INSTM, Via G. Giusti 9, 50121, Firenze, Italy.

[f] Department of Mechanical Engineering Technology, University of Houston, Houston, TX, USA.

[g] Department of Electrical and Computer Engineering, University of Houston, Houston, TX, USA.

[h] Texas Center for Superconductivity (TcSUH), University of Houston, Houston, TX, USA.

[i] Institute of Physical Chemistry, University of Münster, Corrensstraße 28/30, 48149 Münster, Germany.

[l] MEET Battery Research Center, Corrensstraße 46, 48149 Münster, Germany.

Abstract

In this study, self-standing and flexible Li-ion battery negative electrodes made of interconnected two-dimensional carbonized cotton fibers are developed by using a controlled pyrolysis method, and their electrochemical performance in laboratory-scale lithium-based cells is investigated at ambient temperature. By applying this binder- and current collector-free cotton-based carbon fiber electrode, both the Li^+-ion intercalation and capacity decay mechanisms are explored using conventional organic carbonate-based liquid electrolyte. The cotton-based carbon fiber electrode shows excellent cycling performance and delivers a high discharge capacity in the voltage range of 1.5 - 3.0 V. The post cycling analysis of carbon fiber using HR-TEM shows the major SEI layer components formed at the surface of the active fibers during the charge/discharge process. The same electrode is used to assemble a lab-scale Li-ion full cell with high mass loading $LiFePO_4$-based composite electrode, which demonstrates excellent cycling stability, high Coulombic efficiency and remarkable rate capability at ambient temperature.

Keywords: Li-ion battery; controlled pyrolysis; 2D carbon fiber anode; cycling performance; post cycling analysis.

*Corresponding Authors: pravin.jagdale@iit.it, j.nair@fz-juelich.de, claudio.gerbaldi@polito.it

Introduction

There is a positive trend in modern society to establish greener communities, which is being supported with the advocacy to renewable resources, electrified transport, urban gardening and smart architecture, and the use of organic products. Sustainable processes are rapidly growing as a viable alternative to presently used environmentally stress-bearing processes, and there is a massive drive for moving towards bio-based research [1]. Plant-derived materials are one of the promising alternatives, which have been considered to be the only sustainable source of organic carbon on earth [2]. Plant-sourced materials such as rice husk, leaves, banana fibers, tea-leaves and seaweeds have been used as the precursors to prepare carbonaceous materials for pursuing superior structure and property for various energy-related applications [3,4]. Significantly higher electronic conductivity, flexibility, mechanical properties, surface area, and chemical and physical stability are some of the properties that make them more illustrious [5].

It has been predicted that next-generation electronics will be flexible and wearable. Many efforts have been made to develop lightweight, stable, longer lifespan, environmentally safe, and flexible power sources to meet the urgent need for shapeable and wearable electronics [6]. The energy density of the conventional carbon-based electrodes is not high due to its discontinuity in the structure and random pore structure. Two-dimensional graphitic carbon has been recognized as an ideal substrate for high performance energy storage devices [7]. Previous studies already demonstrated its use in the foldable paper-based lithium-ion battery (LIB) with high areal energy density as well as 2D fiber-based electrodes [8-10]. Indeed, graphitic carbon is the preferred active anode material in LIBs [11], being able to reversibly insert/de-insert lithium ions for thousands of charge/discharge cycles, which needs to be considered in addition to its mechanical properties for realizing self-standing electrodes.

Conventional continuous carbon fibers (CFs) have also been widely used because of their excellent capability to allow 1D, 2D and 3D structural orientations [12,13]. Surface and bulk conductivity, and flexibility of CFs permit the integration of high performance and rich functionalities via various chemical reactions [14]. Compared to the conventional CFs, cotton-based carbon fibers (CCF) show enhanced features, chiefly because of the readily tunable hollow structure. It allows having higher active surface area due to intra- and inter-ring layers spaced within the structure, additionally, roughness at the surface of the CCF gives further advantages for specific applications, where surface activity is an important parameter [15]. In addition, CCF shows better electrochemical performance than granular activated carbon due to its continuous fibrous morphology [16].

Cotton is by far the most popular ordinary plant based natural fiber. Commercial cotton, by origin, is made from the soft fiber found in the cotton plant. To make it to the type of textile that we enjoy since many decades, this fiber is spun into a thread or yam, and is most widely used natural-fiber cloth. The creation of CF by pyrolysis of natural cellulose fibers can be traced back to 1883 for electrical-light bulbs; it has been proven to be an exceptional platform for building flexible energy storage devices [17]. Low cost waste management of cotton fiber can serve as a precursor for CCF. Recycling of waste cotton fibers is critical for sustainable raw material availability, however, the resulting product property, the time required to produce, cost, energy consumption, and lack of market demand. In addition to management of resulting waste water are huge challenges to be addressed [18].

Recent studies on CCF from cotton T-shirt have shown an excellent wearable platform for building flexible supercapacitors due to their magnificent flexibility, lightweight, and electronic conductivity [19]. To our knowledge, preparation of the 2D CCFs from waste cotton fibers with

excellent energy storage performance have not been explored to its full potential for application in LIBs, which calls for further work in this area [20]. The development of next-generation of high performing LIBs is slow paced due to the limited capacity provided by the intercalation-type cathodes (cathode limited), where a large portion of the mass is used to accommodate the intercalation of Li^+ ions at the typical ratio of one Li^+-ion per transition metal. The energy density delivered by the graphite-based anodes is also limited, particularly at high current regimes [21]. In addition, supporting composite electrodes onto metallic current collectors does not allow fabrication of flexible and shapeable electrodes. Metallic current collectors in LIBs (e.g., Al and Cu) can also react with common fluorine salt containing electrolyte [22], which causes "corrosion", anodic dissolution, and affects the lithiation/delithiation voltage/potential profiles and the overall cycling stability of the system [23].

In this study, we try to give answers to all of the above reported issues by presenting a rational design for self-standing, flexible and sustainable 2D CCF-based low-cost electrodes that are produced from waste cotton fibers. CCF has two functions; it supports the mechanical integrity of a self-standing electrode and serves as storage material for reversible lithium ion storage. It is observed that during pyrolysis cotton fibers alter their fibrous structure while maintaining their 2D structural orientation in the CCF form. The pyrolyzed 2D CCF after structural orientation helps in designing a beneficial intra- and inter-layer spacing [15] in favor of storing Li^+ ions. The obtained CCF structure is beneficial for Li^+-ion storage, which is supported by the charge/discharge cycling results and cycling rate study in lab-scale cells, both in a cell with lithium metal electrode and in a full cell with $LiFePO_4$-based composite cathode. Hence, this study opens up new directions to innovate electrode design, and actually, even cell architecture by the reuse and revalorization of waste bio-sourced materials.

2. Experimental section

Preparation and characterization of the carbonized cotton fiber cloths

Woven waste cotton fibers with 16 cm^2 (4 cm × 4 cm) dimension were carbonized using controlled pyrolysis process to obtain the 2D CCF. Initially, the sample was cleaned with demineralized water, and then dried in an oven at 70 °C for 4 hours. The carbonization of the sample was carried out under Argon (Ar) atmosphere (100 sccm) with a controlled heating ramp rate of 10 °C min^{-1} up to 800 °C and then kept at that temperature for 30 min.

The structural and thermal properties as well as purity of both the waste cotton fibers and the resulting CCFs were characterized using Thermo Gravimetric Analysis (TGA). The waste cotton fibers were loaded into the TGA (SDT Q600, TA) pan and heated from 30 °C to 800 °C under nitrogen (100 ml min^{-1}) flux. This analysis helped to study the pyrolysis behavior and the transformation of waste cotton fibers to pyrolysed CCFs. An air atmosphere (100 sccm) TGA was performed to study the thermal stability of the as-produced CCFs. In both analyses, the heating ramp rate was set to 10 °C min^{-1}.

The electrical conductivity of the pyrolyzed CCFs was measured with the van der Pauw method by contacting the four corners of a square sample (3.5 × 3.5 mm^2) with small droplets of Ag paste [24]. The resistances of both the vertical and horizontal configurations (R_{ver} and R_{hor}) were acquired by applying a constant current of 1 mA with a Keithley 6221 current source between two corners of a sample and measuring the resulting voltage drop with a Keithley 2182 nanovoltmeter across the opposite two corners of the sample. Possible thermoelectric offsets were removed by the current reversal method. The van der Pauw equation $\exp\left(-\frac{\pi R_{ver}}{R_S}\right) + \exp\left(-\frac{\pi R_{hor}}{R_S}\right) = 1$ was then solved to determine the sheet resistance R_S, and the electrical conductivity was determined as $\sigma = (R_S\, t)^{-1}$, where $t \approx 446\ \mu m$ was the nominal thickness of the sample.

The characteristics in terms of amorphous and graphitized carbon were analyzed using Raman spectroscopy (Renishaw, green laser, λ = 514 nm). The morphology of the CCF samples was characterized by FESEM (ZEISS, Supra-40) analysis. Higher resolution images were taken by coating samples with Cr (~5 nm thick layer), thus avoiding the charging effect during the electron scanning. Specific surface area (SSA) and porous volume were measured by means of N_2 adsorption/desorption isotherms at 77 K (QUANTACHROME Autosorb-1 instrument) on bare CCF piece (2 cm $\times$ 2 cm). Before measurement, the sample was outgassed for at least 15 h at 200 °C to remove water and other atmospheric contaminants. From N_2 isotherms, SSA was measured by Brunauer-Emmett-Teller (BET) multipoint method in the 0.05–0.15 relative pressure range; total porous volume (VT) was measured at p/p^0 = 0.95 [25,26].

High-Resolution Transmission Electron Microscopy analysis (HR-TEM, JEOL 2010) was used to investigate the Li-ion intercalation in/on CCF graphitic planes. The analysis was operated at 200 kV with 0.18 nm resolution. Before taking the TEM images of the post-cycled samples, the electrodes were taken out from the test cells in fully lithiated state. Then, the electrodes were washed with 1:1 w/w EC:DEC solution and dried in vacuum at RT. The samples were further dispersed in ethanol and mixed using a Misonix 4000 sonicator for 20 s; later, this CCF dispersion was dropped over a carbon coated-Cu grid of 300 mesh. The observations presented here correspond to the pristine and lithiated (after discharge) CCF samples. The Fast Fourier Transformations (FFT) and their inverse (IFFT) processes were carried into a Digital Micrograph, and the corresponding simulated microstructures were obtained using VESTA software.

XPS analysis was performed on a PHI Versaprobe Physical Electronics (Chanhassen, MN, USA) equipped with a monochromatic X-ray Al k-α source (1486.6 eV, 15 kV and 1 mA of anodic current).

Preparation of the CCF electrodes and electrochemical characterization

Electrochemical investigations were carried out in 2- and 3-electrode cells. The pyrolysed CCF self-standing electrodes were directly assembled in lab-scale two-electrode cells, using neither current collector support nor binder or conductivity enhancer. Constant current (CC, galvanostatic) cycling at ambient temperature was carried out using 1 cm diameter electrode disks, which were cut from the CCF samples and sandwiched with a glass fiber (Whatman® GF-A, thickness = 200 µm) separator against a lithium metal disk as an other electrode to obtain a lab-scale cell having the CCF‖Li two-electrode cell configuration. In both cases, before assembly, the glass fiber was soaked in the liquid electrolyte solution: 1M $LiPF_6$ in 1:1 v/v EC:DEC (ethylene carbonate: diethyl carbonate) with 2 wt.% of VC (vinylene carbonate) as electrolyte additive (Solvionic, France). The cyclic voltammetry (CV) measurements were carried out in three-electrode Swagelok® cell in which the lithium metal was used as both the counter and the reference electrodes, whereas the CCF was used as working electrode. The same glass fiber soaked in the same liquid electrolyte was used as the separator. The CV measurement was carried out at potentials between –0.02 and 1.2 V vs Li^+/Li at a scanning rate of 0.1 mV s^{-1}. For constant current cycling, cells were continuously charged and discharged in the voltage range of 0.02–1.2 V for rate capability (different current rates from C/20 to 1C), as well as for long-term cycling (1C rate). For cycling stability tests, two-electrode coin cells were cycled using cyclic voltammetry for five cycles. Both capacities and charge/discharge current densities were calculated with respect to the active material weight, viz. 2.5±0.2 mg cm^{-2}, which also represents the total weight of the self-standing electrodes.

A proof-of-concept laboratory-scale 2-electrode Li-ion full cell was fabricated by contacting in sequence the CCF self-supported anode, a layer of Celgard® tri-layer PP/PE/PP separator soaked

in the above detailed liquid electrolyte and a carbon-coated $LiFePO_4$ (LFP/C, BASF) composite cathode film (composition 87:10:3 in LFP:Super-P carbon:CMC, respectively). The assembly was housed in a coffee bag envelope, sealed under vacuum, the electrochemical active area of the laminated coffee bag cell was approximately 10 cm^2, with an active material mass loading of 6.5±0.2 mg cm^{-2} and 2.5±0.2 mg cm^{-2} of LFP and CCF electrodes, respectively. The C-rates were calculated based on the mass loading and theoretical specific capacity of the LFP electrode. Both, CV and galvanostatic cycling experiments were performed on a battery testing system model BT2000 (Arbin Instruments, USA). Clean $LiFePO_4$/C electrodes, separators, lithium metal, and fresh CCF samples were used for electrochemical characterisation. To confirm the results obtained, the tests were performed at least three times on different fresh CCF samples. Electrochemical impedance spectroscopy (EIS, freq. range 300 KHz – 1 Hz, VAC = 20 mV) analysis of both Li metal and Li-ion cell configurations (assembled in ECC-Std cells) was recorded on a VMP3 workstation (Biologic), in three electrode cell configuration including a spectator reference electrode, before and after cycling at ambient temperature. Note that single electrodes are obtained from the same electrode batch of those used in the full cell, but they are not exactly the same electrodes, thus some variations are possible due to limited reproducibility at lab-scale.

3. Results and discussions

Physico-chemical characterization of CCF cloths

   The carbonization of the waste cotton fibers is carried out by pyrolysis under Ar atmosphere at a controlled heating ramp. The resulting CCF cloth after the carbonization process is shown in **Fig. 1a**, where the good retention of mechanical integrity and shape are well confirmed for a material free of visible formation defects. CCF cloth can be easily folded, demonstrating that, even after

carbonization, the material is self-standing, can be handled and shaped as conventional paper sheets. The morphology and the fiber microstructure is investigated using FESEM analysis, which demonstrates a porous and twisted fiber morphology for the CCF samples, as shown in **Fig. 1b** and **1c**. The average thickness of individual fiber is 5±0.5 µm, as evidenced in **Fig. 1c**.
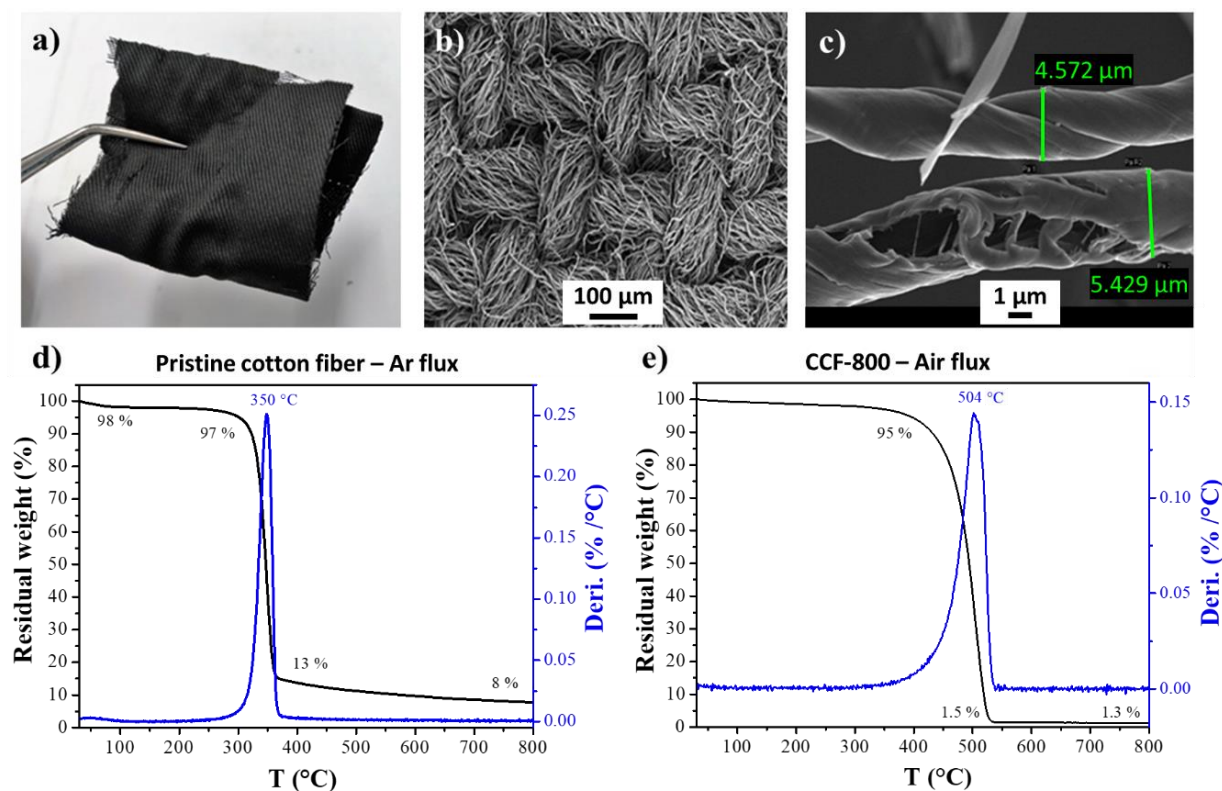

Figure 1. a) Digital photographs of CCF fiber in bending mode. FESEM images of b) the CCF surface overview and c) separated single strands of fiber showing the porous and twisted structures. TGA and corresponding DTG profiles of d) pristine cotton fiber under nitrogen flux, and e) pyrolysed CCF sample at 800 °C under air flux.

The weight loss can be used to investigate the purity and thermal stability of carbon/cotton fibers. Indeed, this method also helps in studying the conversion of waste cotton fibers to carbon fiber during the carbonization process. Hence, as a preliminary investigation, the TGA technique is

applied to determine the threshold decomposition temperature, which is indicated by the starting point of the weight loss [27].

The initial weight loss (2 wt.%) during the heating step is observed between 30 and 100 °C (**Fig. 1d**), which corresponds to dehydration or moisture loss from the cotton cellulose, and this loss does not impart any adverse effect on the strength of the cotton fibers [28]. However, dehydration of the cellulosic units leads to the formation of intermediates with double-bonds [29]. Noticeably, the mass change in fibers starts by a lowering of molecular weight. Until 300 °C, a limited mass loss of < 3 wt. % is observed due to thermochemical oxidation reaction in the polymeric structure of cotton fibers. After 300 °C, the rate of residual mass loss is increased considerably. The carbonization reaction starts at 300 °C with a significant material weight loss of 84 wt.% followed by second minor weight loss of 5 wt. % up to 800 °C. From the first derivative of the thermos gravimetric (DTG) profile, the major weight loss is observed at 350 °C. Considering the thermal profile from the TGA analysis, it can be assumed that the carbon microstructure may be formed between 300 and 500 °C [30]. The degradation of the cellulosic polymer chain to monosaccharide derivatives occurs during the carbonization process. The intermediates form aromatic structures by releasing various types of gases that contain noncarbonated atoms (O, H). Additionally, the carbonaceous material is converted into more ordered layers of carbon through the heat treatment between 500 to 800 °C. Indeed, the pyrolysis of cotton fibers up to 800 °C causes the formation of carbon fiber residue of 8 wt.%. The full mechanism of aromatization related to the graphitic products is rather complex and not fully understood due to the sophisticated characterization of the cellulose decomposition and the existence of many competing reactions at the different stages of carbonization [31]. Hence, an optimal compromise between energy consumption (during

pyrolysis) and resultant degree of graphitization / mechanical properties is necessary to obtain high performing carbon materials for LIBs [32].

The CCFs produced at 800 °C under Ar atmosphere are further analyzed for understanding their overall structural characteristics using TGA analysis under air flow. The results (**Fig. 1e**) show that the CCF is thermally stable up to 400 °C and only 5 wt. % of weight loss is observed until 400 °C, afterwards, a sudden and major weight loss is initiated. Generally, less ordered carbon materials contain large amount of oxidation active sites characterized by low activation energy for the oxidation reaction [33]. The major weight loss (~93 wt.% of the overall loss) is observed in the range of 380-540 °C, with maximum at 504 °C, as commonly observed for partially graphitized carbon materials. The inorganic residue in the form of ash observed at the end of the TGA corresponds to 1.3 wt.%.

The carbonization as well as the graphitic nature of the CCFs are further confirmed by Raman spectroscopy analysis (**Fig. 2a**). The CCF material shows an amorphous behavior in D (D-peak at ≈ 1350 cm^{-1}) and G (G-peak at ≈ 1600 cm^{-1}) zones. The 2D zone (2200-3400 cm^{-1}) clearly shows the presence of three distinct peaks, although enlarged in width and merged. The presence of a relevant number of not-fully coordinated sp^2 sites is witnessed by the D peak intensity, width, and its D+G peak relevance. The clear separation between the D and the G peaks pointing towards the presence of partially ordered microstructures and this assessment is further supported by the 3-peak 2D structure [34]. Additionally, carbonization of CCF is also confirmed by the adherence of the D+G region to the results previously obtained on similar bio-char materials, which had been structurally investigated in more detail; overall, the Raman spectra is a typical example of a carbonized biochar [35]. The electrical conductivity measured at 25 °C by the four-point van der Pauw method (see Fig. S1 in supplementary material) was observed to be 1.077 Ω^{-1} cm^{-1}.

The BET specific surface area (S.S.A.) and the total pore volume of the CCF material are measured from N_2 isotherm (**Fig. 2b**), resulting in values of 46 m^2 g^{-1} and 3.6×10^{-2} cm^3 g^{-1}, respectively. It should be noted that the open hysteresis loop form of the curve indicates diffusion limitations likely occurred during N_2 adsorption at 77 K despite we applied long equilibration time (*i.e.*, 10 min for each isotherm point) for the measurement.
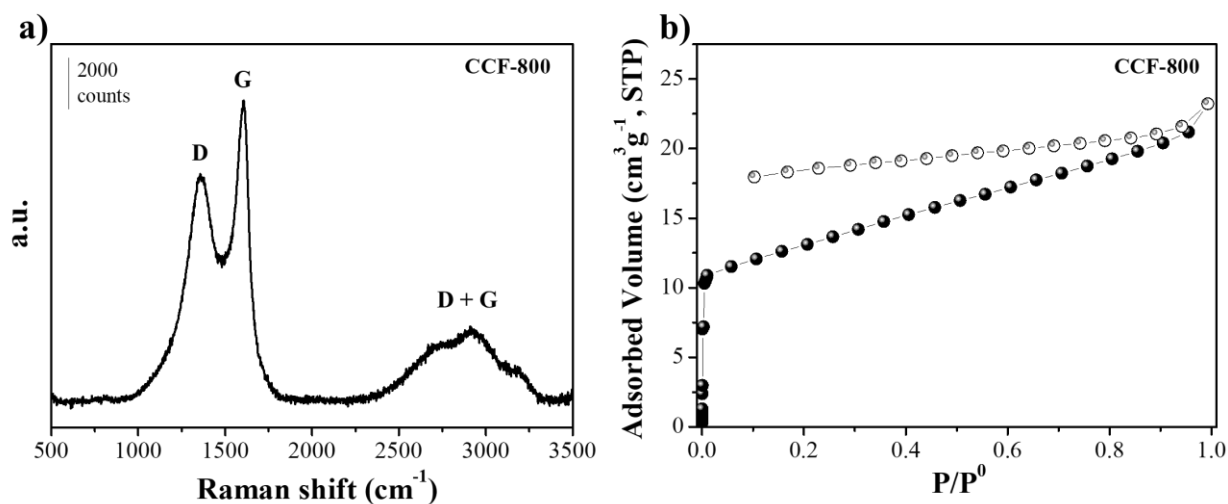

Figure 2. a) Raman spectroscopy analysis and b) N_2 adsorption/desorption isotherm at 77 K of CCF sample.

We found a similar open loop behavior for other cotton-derived carbon materials [36]. Such diffusion limitations commonly occur within ultra-micropores (i.e., pore width < 0.7 nm) of porous carbon materials, which are hardly accessible to N_2 at 77 K [25], and hinder the correct use of any model (e.g., BJH or NLDFT) for the measurement of Pore Size Distributions. However, given the isotherm shape, it is reasonable to assume that most of the porous volume of CCF is made of ultra-micropores.

Electrochemical characterization in Li-based half- (Li metal) and full- (Li-ion) cells

For the evaluation of the electrochemical behavior, the as-prepared, self-standing and self-supported CCF electrodes are directly assembled into three-electrode Swagelok cells with 2 wt.% VC-added liquid organic carbonate-based electrolyte, as detailed in the experimental section. The loading weight of the CCF electrode is 2.5 ± 0.2 mg cm^{-2}. The ambient temperature electrochemical behavior overview is shown in **Fig. 3**. The CCF electrodes are initially tested for cyclic voltammetry in a three-electrode Swagelok$^{\circledR}$ cell with Li metal as both the counter and the reference electrodes. Typical cyclic voltammograms obtained at a scan rate of 0.1 mV s^{-1} between 0.02 and 1.2 V vs. Li^{+}/Li are shown in **Fig. 3a**. The shapes and potentials of the cathodic and anodic peaks are generally consistent with the results reported in literature for the typical reduction and following oxidation of carbon to progressively form the intercalation compound with lithium ions [37]. At potential values below 0.15 V vs. Li^{+}/Li, several peaks related to various stages of carbon reduction or oxidation are detectable; peaks are rather sharp, likely ascribed to the Li^{+}-ion intercalation/deintercalation into/from the homogeneous structure of ordered crystalline graphite platelets. The separation between those peaks is very limited, accounting for a partially amorphous structure of the CCF self-supported electrode. Pseudocapacitive Faradaic behaviour is predominant at higher potential values. Pseudocapacitance is generally proposed to arise at the electrode surfaces where materials undergo fast and reversible redox reaction. It reflects a Faradaic process that takes place on the surface or near-surface of the electrode materials, and the related materials are considered as "pseudocapacitive materials" [38]. This is common for carbon materials having a turbostratic structure, where two different structures, i.e. ordered structure and disordered structure, may coexist.
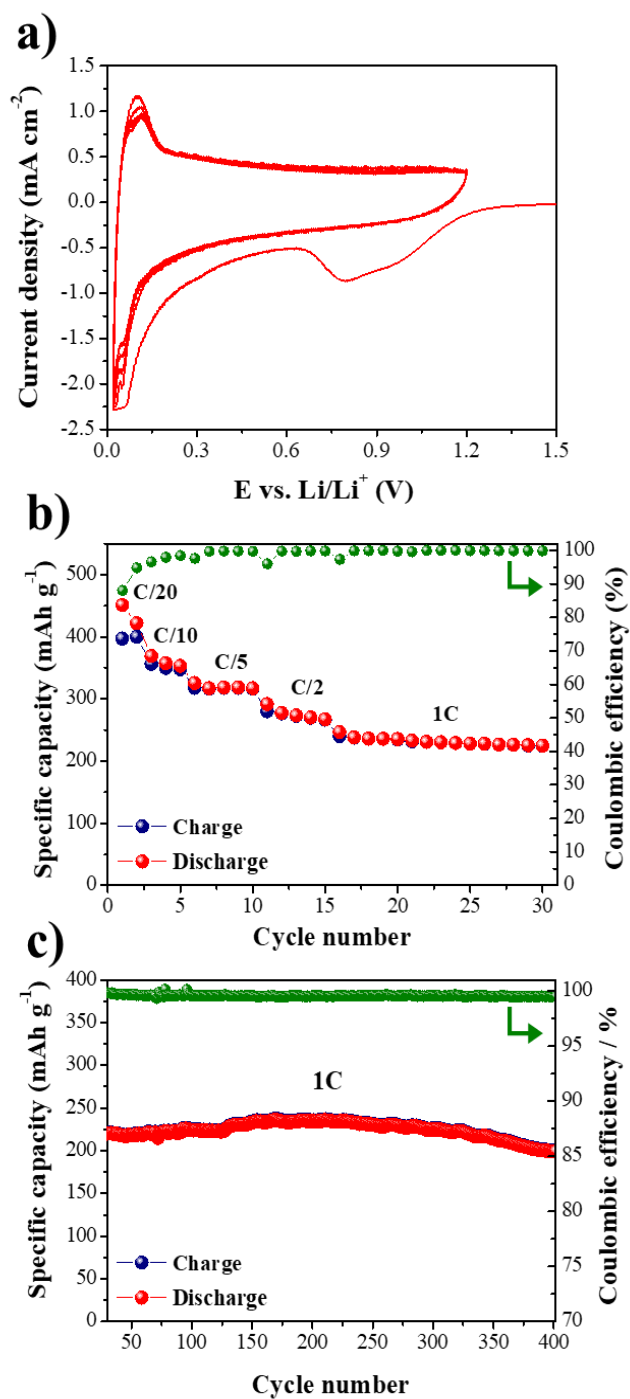
Figure 3. Ambient temperature electrochemical behavior of CCF electrodes in lab-scale Li-metal cells with 1M LiPF$_6$ in EC:DEC (2 wt.% VC) electrolyte: a) Cyclic voltammetry of the CCF-based three electrode cell, at RT. Galvanostatic cycling of the CCF based cell at b) different current rates and c) at 1C for 400 cycles. The loading weight of the CCF electrode was 2.5±0.2 mg cm^{-2}.

Conversely to an ordered stack of microcrystallites in highly conductive graphene layers, a disordered structure made of randomly organized microcrystallites contains internal vacancies where large amounts of lithium ions can be accommodated. [39,40]. In general, these are carbonaceous materials obtained by heat-treatment at low temperature (generally, below 1000 °C) and the presence of disordered structures and defects accounts for a non-uniform distribution of voids and free spaces for the reversible reaction with lithium ions [40]. In their CV profiles, some signals of carbon oxidation/reduction falling at different potentials is likely, which is ascribed to different structural situations of the carbon matrix, giving rise to enlarged peaks with large overpotential as for the behaviour above 0.2 V, corresponding to the reduction-oxidation of carbon in the disordered accommodation vacancy.

Overall, the cyclic voltammetry response is highly reversible and rather stable, as well-evidenced by the very similar Li^+-ions insertion/de-insertion capabilities and the quasi-superposition of the potential values of the oxidation/reduction peaks upon reversible cycling. The broad peak appearing in the first cathodic scan between 1.2 and 0.6 V vs. Li^+/Li can be ascribed to the formation of the solid electrolyte interphase (SEI) due to the decomposition of electrolyte components on the surface of the electrode [41]; the peak is clearly observable only in the first cycle and, then, it disappears in the following. It represents the expected side reaction with the components of the electrolyte, which causes the irreversible capacity loss during the first cycle (**Fig. 3b**), and it also includes the reduction of VC additive molecules [42]. In the side reaction, solvent molecules and salt anions are reduced on the active material surface, thus forming an hardly soluble protecting surface film (SEI formation), which prevents further reactions between the components of the electrolyte and the carbonaceous active material including related graphite exfoliation [43,44].

The galvanostatic cycling of the two electrode cell with the VC containing liquid electrolyte is shown in **Fig. 3b** (rate capability test) and **Fig. 3c** (long-term cycling at 1C rate). Several previous works reported that a turbostratic structure is desirable in lithium-based cells conceived for high rate applications [45,46], thus the rate capability is first examined in order to evaluate the capability of the CCF electrode to avoid noticeable specific capacity decay at increasing current regimes. **Fig. 3b** clearly shows that the CCF-based cell delivers specific capacity values of about 449 and 398 mAh g^{-1} during first charge (Li^+ intercalation) and discharge (Li^+ deintercalation) steps, respectively. This noticeable difference in specific capacity values during initial cycling is ascribed to the expected side reaction with the components of the electrolyte and SEI formation, as discussed previously for CV. Nevertheless, the CCF electrode demonstrates rather limited initial irreversible capacity loss, which is important for practical application in full Li-ion cells. In general, the CCF self-supported electrode shows very good rate capability, with relatively low capacity drop while progressively increasing C-rate from C/20 to 1C and, at each selected current rates, its cycling behavior is very stable. Specific capacity decay at increasing current rates is generally ascribed to limitations in Li^+-ion diffusion and the electron transport through the active material grains; as a result, we can say that cotton fibers are well-suited waste source material to obtain high performing carbonaceous LIB anodes. The good rate capability also confirms a predominant pseudocapacitive Faradaic behavior, the rate of which is not limited by solid-state diffusion of Li^+-ions in a broad interval of scan rates. The reversible specific capacity at 1C rate after 30 cycles is found to be higher than 225 mAh g^{-1}, which means only about 40% lower than the theoretical limit for a graphite electrode (i.e., 372 mAh g^{-1} [47]). This is remarkable for a bare, self-supported electrode cycled at high 1C rate and, without binders and conductivity enhancers. After the first cycle, the Coulombic efficiency rapidly increases to above 99% and, subsequently,

remained highly stable throughout cycling, actually approaching 99.8% indicating that the use of VC as additive is effective: the formed SEI film remains intact and shows good reversible cycling after the surface reactions are completed.

Eventually, the electrochemical behavior of the CCF-based electrode is evaluated in terms of long-term cycling performance to confirm the stability of the carbonaceous structure upon prolonged and continuous reversible intercalation/deintercalation cycles of Li^+-ions at 1C current rate. **Fig. 3c** shows that the CCF-based anode is capable of maintaining rather stable specific capacity values well in excess of 200 mAh g^{-1} up to 400 cycles, thus demonstrating to be highly stable even in the absence of binders and conductivity enhancers. The reversible capacity after 400 cycles at C/10 was found to be about 203 mAh g^{-1}, which corresponds to approximately 90% retention of the reversible capacity at the same rate after 30 cycles. In addition, the Coulombic efficiency kept steady for more than 99.8% indicating an optimum reversibility. Overall, the obtained results show that the use of carbonized cotton fibers in the form of self-standing and self-supported electrodes lead to stable electrochemical behavior upon prolonged cycling and remarkable performance, in particular when increasing the current regime. Interestingly, the self-supported CCF electrodes are hereby tested in their "as-prepared" form (i.e., 100 wt.% active material, which, on an industrial perspective means enhanced overall energy density of the final device), viz. without the addition of any electronic conductivity enhancers and/or binders. Additionally, the electrochemical performance is highly valuable even at 1C discharge/charge current regimes, with about 20% lower specific capacity output when compared to state-of-the-art commercial and crystalline graphite and/or hard carbon electrodes from major companies, like Imerys Graphite & Carbon (formerly TIMCAL), Hitachi and SGL Carbon [32]. We also stress the fact that no activating agent

(e.g., KOH) is here used to increase SSA, which enhances the simplicity and scalability of the electrode material preparation.

The cycled samples from these cells are analyzed using high-resolution transmission electron microscopy to investigate the Li-ion intercalation in/on graphitic planes of CCF. HRTEM micrographs are shown in **Fig. 4**, which are divided in the following three sets of images: the carbon substrate (**Fig. 4a**), the sample after first charge (lithiation, **Fig. 4b**) and the sample after five charge/discharge cycles (**Fig. 4c**). The regions in the white squares (dotted lines) represent the magnified insets on the right side images that are used for in depth analysis using FFT and IFFT in the Digital Micrograph software, and here we only presented the IFFT processed images. Based on the HRTEM image in **Fig. 4a**, one can conclude that the raw CCF sample is majorly composed of amorphous carbon. The edge structure of the 2D carbon is an important information and HRTEM image, also supported by FESEM, confirms that the edges of the CCF are of open structure or formed by closed shells. As the fibers are a part of a woven fabric, the contacts between the fibers are similar to a textile fabric, as shown in the FESEM and digital images. Indeed, EDX measurements confirmed that there is no Co or other transition metals present in the fibers. Indeed, contaminants or doping atoms are an issue in end-of-life cotton and such metals influence the properties of carbon formed after pyrolysis [48]. For this reason, we performed XPS survey analysis (see spectra in Fig. S2 in supplementary material), which detected only C, O and Ca related peaks. No other peaks detected, even if other atoms are present, they are below the XPS level of detection (i.e., a few %, depending on the atom). Thus, it can be confirmed that the cotton fiber used and the CCF formed after pyrolysis have a high degree of purity.

In the cycled sample (**Fig. 4b**), we can observe the carbon substrate particles supporting lithium-rich domains. The lithium rich particles are homogeneously distributed and have sizes between 3.5

and 10 nm. The respective image shows a closer look of the lithium particles where the highly crystalline particles are observed showing that their nature is mainly Li_2CO_3.
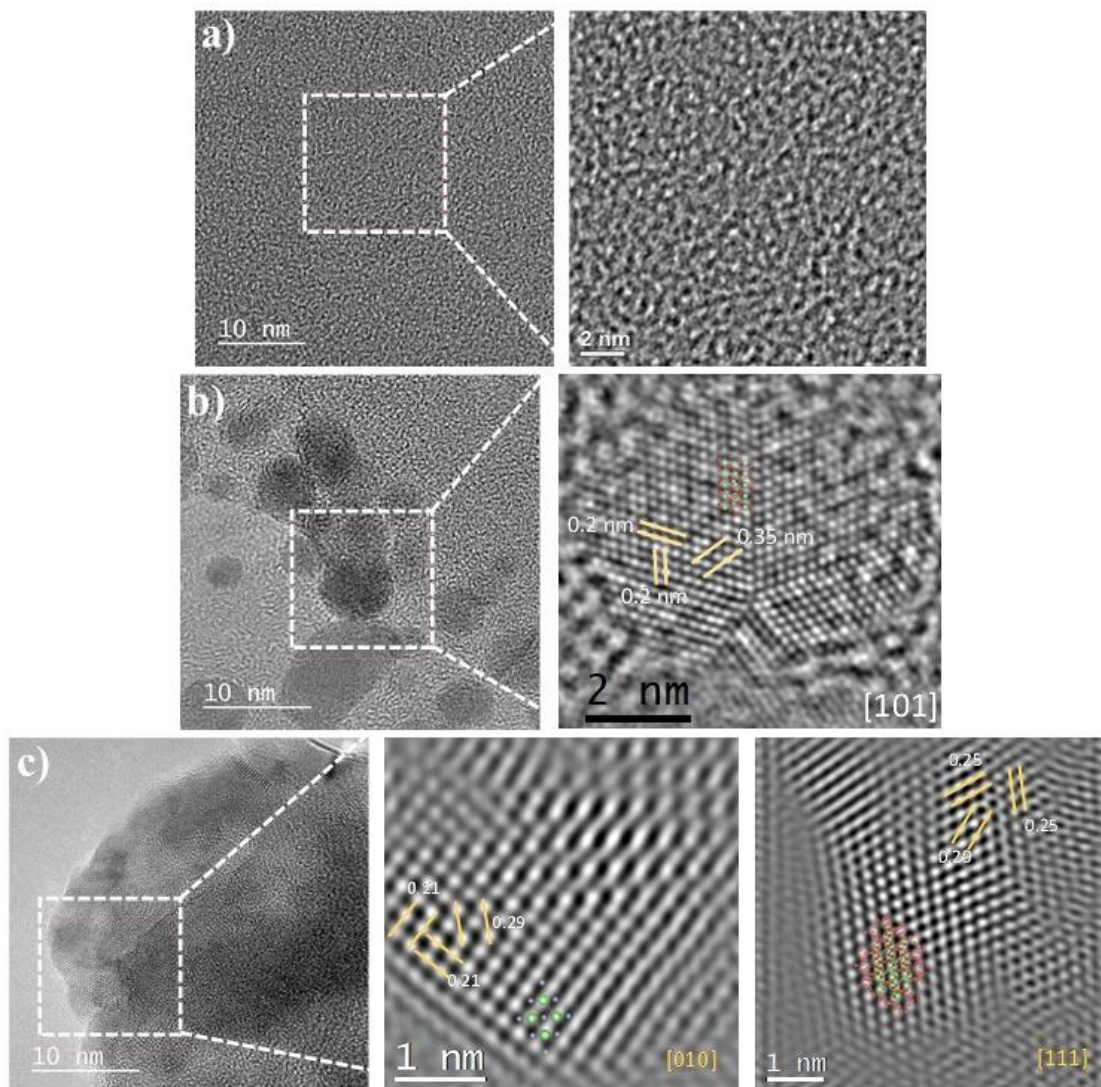

Figure 4. HR-TEM of the a) bare CCF electrode, b) CCF with the lithium particles (Li_2CO_3) after the first charge (lithiation), and c) the CCF electrode with lithium particles (Li_2CO_3 and LiF) after five charge/discharge cycles. Notice the location of the Li_2CO_3 particles that move from the center of the substrate to the edges or surface.

The respective d-spacing are provided in **Fig. 4b** for the identified planes and correspond to (111) = 0.35 nm, (101) = 0.2 nm giving a projection image along the zone axis (101). The Li_2CO_3 structure corresponds to the space group 15 also identified as C 2/c that is monoclinic. Additionally, we have found Li_2O_2, which corresponded to a previously proposed phase. The Li_2O_2 has a space group P1 (hexagonal) with lattice constants of a = b = 0.32 nm and c = 0.77 nm [49]. The d-spacing of the identified particles is 0.24 nm and is characteristic of the family of (101) and 0.4 nm is attributed to the (002) resulting in a zone axis along the (010) direction. The STEM and EELS analyses of this sample are challenging, and in both methods, the lithium particles move away from the analyzed region dispersing homogeneously along the carbon substrate. During this process, the lithium-rich particles are no longer observable; instead, one can only see a homogeneous dispersion of lithiated compounds. In EELS, the electron beam charges the sample and lithium migrates away from the field of view. HRTEM is performed with lower electron dose allowing a limited Li diffusion.

In the CCF sample after five charge/discharge cycles (**Fig. 4c**), the lithium-rich particles transform from semi-spherical into regular particles (squares or tetrahedrons). Furthermore, in some portion of the cycled sample, we find randomly distributed Li-rich particles along the substrate. These particles go from concentrated within the substrate to surface agglomerates. Moreover, after the charge discharge process, it is also observed that the Li-rich particles migrate to the substrate (carbon) surface and they are no longer randomly distributed. However, they form agglomerates of 3-10 nm size, where their crystallinity changes drastically. Indeed, these particles transform from a highly crystalline particle to a shorter and smaller domains having limited crystallinity and higher density defects. Based on the HRTEM analysis performed, the major lithium particles that are identified on the galvanostatically cycled sample as LiF and Li_2CO_3 [50]. The LiF has a rock

salt structure, while the Li_2CO_3 transforms from monoclinic to the P1 space group. This selection is made based on the similarity with the chemistry used on references [49,51] and the present one. Based on the HRTEM analysis, it can be said that Li_2CO_3 is transformed completely from monoclinic to triclinic. Li_2CO_3 has a space group P1 (trigonal) with lattice constants of a = b = 4.91 nm and c = 6.35 nm [49]. The d-spacing of the identified particles is 0.25 nm and is characteristic of the family of (110). The second d-spacing is d = 0.245 nm and identified as 0.25 nm and corresponds to the (121) family of planes, and finally, the third one is 0.29 nm that attributes to the (112) family. The difference among the theoretical and experimental d-spacing is approximately 2%, which is within systematic error considerations. The calculated zone axis for the Li_2CO_3, Li_2O_2 and LiF particles are (101), (010) and (110) direction, respectively.

Lithium is generally intercalated within the interlayer gaps of graphite, during direct contact and cathodic polarization [52]. As side reaction, electrolyte decomposition takes place and the type of electrolyte decomposition products will depend on the type of electrolyte used. For example, there are possibilities for lithium carbonate, lithium fluoride, lithium formate, lithium hydroxide and peroxide, etc. These products may be precipitated over the surface as solid electrolyte interphase (SEI) layer. Then there will be various organic products that are formed due to the decomposition of organic carbonates that are used to make electrolytes [53]. In our case, we have also used VC as an additive, which is known to form a polymeric layer during the initial charge discharge cycles [54]. However, this polymeric layer is not clearly identifiable using HRTEM as the focused ion beam decomposes the polymeric layer on the CCF substrate [55,56]. Hence, one may speculate that one of the reasons for the lower Coulombic efficiency in the first cycle may arise from a thick SEI layer that is mainly composed of Li_2CO_3 (monoclinic) and Li_2O_2 formed on the CCF surface during the first charge.

Here, the self-standing 2D CCF electrode could not only improve the reaction kinetics through a porous and conductive network but also avoid the influence of current collector and other components (e.g. binder) on performance. The electrochemical performance of the 2D CCF electrode is tested under different voltage ranges in conventional electrolyte. It is found that by controlling the testing voltage in the range of 1.5-3.0 V (vs. Li^+/Li) is possible to limit the amount of inserted lithium. The reaction involving the production of Li-C and its associated volume changes is restrained so that the electrode could be steadily cycled in the organic carbonate solvent based electrolyte with reasonably high specific capacity output even at higher current regimes.

To confirm the promising prospects of the CCF self-supported electrode to be used in close-to-real two-electrode cell configuration, we coupled it with a $LiFePO_4$-based composite electrode (6.5 mg cm^{-2} active mass loading of LFP) and assembled a proof-of-concept lab-scale Li-ion cell. It is tested at ambient temperature for its specific capacity output and rate capability at different current regimes using the same VC-added liquid organic carbonate-based electrolyte as for the half-cell shown in Figure 3. Cycling results are shown in **Figure 5**, which displays the constant current behavior of the LFP∥CCF Li-ion full cell in terms of specific capacity vs. cycle number at different current regimes (from C/10 to 1C) and representative galvanostatic charge/discharge profiles (2nd cycle, at C/10 rate). The proof-of-concept results are very interesting: the voltage drop in passing from charge to discharge is found to be small (inset of **Figure 5**), which means a low internal resistance of the cell. Overall, the LFP∥CCF Li-ion cell shows good rate capability up to 1C rate and, after the initial activation cycles at low C/10 rate, operates at excellent Coulombic efficiency (i.e. above 99.3%), which is fundamental for successful long-term operation. The output in terms of specific capacity values, being proof-of-concept results, is remarkable (viz., >120 mAh g^{-1} at

C/10; > 110 mAh g^{-1} at C/5; > 100 mAh g^{-1} at C/2; and 90 mAh g^{-1} at 1C rate), the cell showing

stable cycling at each of the tested rates and overall good capacity retention.
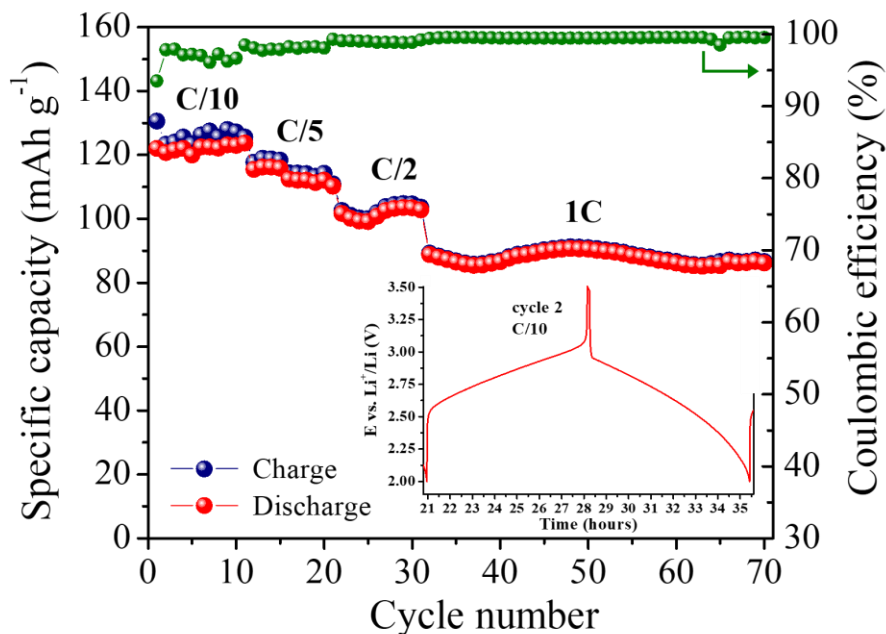

Figure 5. Ambient temperature electrochemical behavior (galvanostatic cycling) of the lab-scale

Li-ion cell assembled with CCF self-standing anode and a standard composite LFP cathode in 1M

LiPF$_6$ in EC:DEC (2 wt.% VC) liquid electrolyte: plot of specific capacity vs. cycle number at

different current rates (from C/10 to 1C calculated vs. the theoretical specific capacity of the LFP

electrode, mass loading 6.5±0.2 mg cm^{-2}). The inset shows representative charge/discharge

potential vs. time profiles of the Li-ion cell extracted from the galvanostatic cycling.

EIS analysis was carried out on the LFP/CCF Li-ion full cell, in three electrode cell configuration

including a spectator reference electrode, before and after cycling at ambient temperature. Data

are shown in the form of Nyquist plots in Fig. S3 in supplementary material and also compared

with the Nyquist plots of the single electrodes tested in Li metal cell configuration (details in

experimental). As expected, the electrochemical evaluation of the separate electrodes shows

different effects on CCF and LFP upon cycling (see plot a and b in Fig S3, respectively, in supplementary material). Both the electrodes show an increase of the mid frequency semicircle, with a shift of real impedance towards lower frequency values, while at high frequencies no large shift is observed. The initial CCF electrode impedance is overall much smaller than the LFP impedance, but the semicircle becomes much larger while cycling, which accounts for large electrolyte decomposition and resistive surface film (SEI) formation during cycling, as observed by HR-TEM; conversely, for the LFP electrode the semicircle (broadened) amplitude increase is much more limited and, towards low frequencies, all spectra have similar shape with only some minor variation in magnitude and lower angle of the tail after the mid frequency semicircle, as electrolyte resistive films on the nanosized active material particles is limited with limited increase of the intercalation resistance during reversible lithiation process. The Li-ion full cell EIS analysis shows typical dominant cathode impedance, as the increase of charge transfer resistance is mainly contributed by the LFP/electrolyte interface [57], while the CCF/electrolyte interface chiefly contributes in the low frequency range to the solid-phase diffusion resistance. Overall, minor variation in overall resistance as well as shape and size of the profiles is observed, with negligible shift in high frequency intercept (chiefly ascribed to the combined resistance of this and the separators), thus no ohmic potential drop and rather limited real impedance increase at lower frequency values, which well matches with the stable full cell cycling shown in Fig. 5.

The results shown in the present work and, in particular, the LFP‖CCF proof-of-concept Li-ion cell cycling response put in evidence the promising prospects of our newly proposed CCF self-standing electrode obtained by controlled pyrolysis of waste cotton T-shirt. Direct comparison with literature results is challenging due to the scarcity of works focused specifically on waste cotton fibers, their carbonisation and demonstration in lab-scale LIBs. However, literature reports

addressing pyrolysis-based electrode preparation from various other materials and related carbon fibers in different battery chemistries are present [58-62], which may be referred to the reader for more information. Overall, the proposed self-standing CCF has attracting properties for achieving successful adaptation in secondary Li-ion cells directed to high-energy, robust and shapeable energy storage applications.

Conclusions

In summary, we have developed a self-standing CCF electrode with interconnected two-dimensional carbonized cotton fibers directly obtained by simple controlled pyrolysis of waste cotton T-shirt. Cotton cloth maintains its robustness due to the interconnected 2D structure, handling ability and self-standing features even after carbonization, which postulates its use in flexible/wearable devices. The CCF material shows typical characteristics of disordered carbon, having a limited degree of graphitization, with small graphitic domains randomly organized in an amorphous matrix and high temperature thermal stability in air.

The CCF electrode is directly assembled in lab-scale Li-metal cells with vinylene carbonate-containing organic carbonate liquid electrolyte, both for rate capability up to 1C rate and for long-term cycling up to 400 cycles at 1C rate at ambient temperature. The same electrode is also assembled in lab-scale Li-ion full cell with high mass-loading LiFePO$_4$-based composite electrode demonstrating optimal profiles, excellent cycling stability and coulombic efficiency and remarkable rate capability at ambient temperature. It is worth noticing that, in all cases, the self-supported CCF electrodes are hereby tested in their "as-pyrolysed" form, which means 100 wt. % of carbonaceous active material without addition of any binders and/or electronic conductivity enhancer which, on an industrial perspective, means enhanced overall energy density of the final

device. In addition, no activating agent is used to increase SSA, which accounts for easiness and scalability of material production. Post-cycling analysis by TEM was helpful to investigate the Li-ion intercalation in/on graphitic planes of CCF and homogeneity of lithium domains in the active electrode material. The Li-rich phases change from Li_2CO_3 in the only discharged sample to Li_2CO_3 and LiF after the charge discharge process, particularly, Li_2CO_3 changes from monoclinic to triclinic with smaller crystalline domains and particle size.

Overall, the use of CCF in the form of a self-standing, self-supported electrodes leads to stable electrochemical behavior upon prolonged cycling and remarkable performance even at 1C rate, which, combined with the high mechanical properties thanks to the interconnected two-dimensional carbonized cotton fiber structure supports for their use in next-generation energy storage devices for flexible/wearables smart electronics.

Notes

The authors declare no competing financial interest.

Acknowledgements

References

[1]   L.A. Lucia, Lignocellulosic biomass: A potential feedstock to replace petroleum, BioResources 3 (2008) 981–982. https://doi.org/10.15376/biores.3.4.981-982.

[2]   G.W. Huber, S. Iborra, A. Corma, Synthesis of Transportation Fuels from Biomass: Chemistry, Catalysts, and Engineering, Chem. Rev. 106 (2006) 4044–4098. https://doi.org/10.1021/cr068360d.

[3]   S. Bhardwaj, S. V Jaybhaye, M. Sharon, D. Sathiyamoorthy, K. Dasgupta, P. Jagadale, A. Gupta, B. Patil, G. Ozha, S. Pandey, T. Soga, R. Afre, G. Kalita, M. Sharon, Carbon Nanomaterial from Tea leaves as an Anode in Lithium Secondary Batteries, Asian J. Exp. Sci. 22 (2008) 89–93.

[4]   S. Dühnen, J. Betz, M. Kolek, R. Schmuch, M. Winter, T. Placke, Toward Green Battery Cells: Perspective on Materials and Technologies, Small Methods. 4 (2020) 2000039. https://doi.org/10.1002/smtd.202000039.

[5]   M. Srivastava, J. Singh, T. Kuila, R.K. Layek, N.H. Kim, J.H. Lee, Recent advances in graphene and its metal-oxide hybrid nanostructures for lithium-ion batteries, Nanoscale 7 (2015) 4820–4868. https://doi.org/10.1039/C4NR07068B.

[6]   H. Gwon, J. Hong, H. Kim, D.-H. Seo, S. Jeon, K. Kang, Recent progress on flexible lithium

rechargeable batteries, Energy Environ. Sci. 7 (2014) 538–551. https://doi.org/10.1039/C3EE42927J.

[7]   R. Raccichini, A. Varzi, S. Passerini, B. Scrosati, The role of graphene for electrochemical energy storage, Nat. Mater. 14 (2015) 271–279. https://doi.org/10.1038/nmat4170.

[8]   L. Zolin, J.R. Nair, D. Beneventi, F. Bella, M. Destro, P. Jagdale, I. Cannavaro, A. Tagliaferro, D. Chaussy, F. Geobaldo, C. Gerbaldi, A simple route toward next-gen green energy storage concept by nanofibres-based self-supporting electrodes and a solid polymeric design, Carbon N. Y. 107 (2016) 811–822. https://doi.org/10.1016/j.carbon.2016.06.076.

[9]   T.H. Nguyen, A. Fraiwan, S. Choi, Paper-based batteries: A review, Biosens. Bioelectron. 54 (2014) 640–649. https://doi.org/10.1016/j.bios.2013.11.007.

[10]   G. Meligrana, S. Ferrari, L. Lucherini, J. Celè, F. Colò, J. Brugger, C. Ricciardi, R. Ruffo, C. Gerbaldi, $Na_3V_2(PO_4)_3$ -Supported Electrospun Carbon Nanofiber Nonwoven Fabric as Self-Standing Na-Ion Cell Cathode, ChemElectroChem. 7 (2020) 1652–1659. https://doi.org/10.1002/celc.202000345.

[11]   R. Schmuch, R. Wagner, G. Hörpel, T. Placke, M. Winter, Performance and cost of materials for lithium-based rechargeable automotive batteries, Nat. Energy. 3 (2018) 267–278. https://doi.org/10.1038/s41560-018-0107-2.

[12]   S. Gorgutsa, J.F. Gu, M. Skorobogatiy, A woven 2D touchpad sensor and a 1D slide sensor using soft capacitor fibers, Smart Mater. Struct. 21 (2012) 015010. https://doi.org/10.1088/0964-1726/21/1/015010.

[13]   E. Archer, S. Buchanan, A. McIlhagger, J. Quinn, The effect of 3D weaving and consolidation on carbon fiber tows, fabrics, and composites, J. Reinf. Plast. Compos. 29

(2010) 3162–3170. https://doi.org/10.1177/0731684410371405.

[14] N. Padmanathan, S. Selladurai, Controlled growth of spinel $NiCo_2O_4$ nanostructures on carbon cloth as a superior electrode for supercapacitors, RSC Adv. 4 (2014) 8341–8349. https://doi.org/10.1039/C3RA46399K.

[15] P. Jagdale, E.P. Koumoulos, I. Cannavaro, A. Khan, M. Castellino, D.A. Dragatogiannis, A. Tagliaferro, C.A. Charitidis, Towards green carbon fibre manufacturing from waste cotton: a microstructural and physical property investigation, Manuf. Rev. 4 (2017) 10. https://doi.org/10.1051/mfreview/2017008.

[16] K. Leitner, A. Lerf, S. Villar-Rodil, F. Suárez-García, A. Martínez-Alonso, J.M.D. Tascón, Nomex-derived activated carbon fibers as electrode materials in carbon based supercapacitors, J. Power Sources 153 (2006) 419–423. https://doi.org/10.1016/J.JPOWSOUR.2005.05.078.

[17] L. Hu, M. Pasta, F. La Mantia, L. Cui, S. Jeong, H.D. Deshazer, J.W. Choi, S.M. Han, Y. Cui, Stretchable, Porous, and Conductive Energy Textiles, Nano Lett. 10 (2010) 708–714. https://doi.org/10.1021/nl903949m.

[18] F.K. Tamer, E.D. Mohamed, Recycling of Textiles, J. Text. Sci. Eng. S2 (2014) 1–2. https://doi.org/10.4172/2165-8064.S2-001.

[19] Z. Gao, N. Song, X. Li, Microstructural design of hybrid CoO@NiO and graphene nano-architectures for flexible high performance supercapacitors, J. Mater. Chem. A. 3 (2015) 14833–14844. https://doi.org/10.1039/C5TA03057A.

[20] P.G. Bruce, S. a. Freunberger, L.J. Hardwick, J.-M. Tarascon, $Li-O_2$ and Li-S batteries with high energy storage, Nat. Mater. 11 (2011) 172–172. https://doi.org/10.1038/nmat3191.

[21] J. Betz, G. Bieker, P. Meister, T. Placke, M. Winter, R. Schmuch, Theoretical versus

Practical Energy: A Plea for More Transparency in the Energy Calculation of Different Rechargeable Battery Systems, Adv. Energy Mater. 9 (2019) 1803170. https://doi.org/10.1002/aenm.201803170.

[22] S. Nowak, M. Winter, Chemical Analysis for a Better Understanding of Aging and Degradation Mechanisms of Non-Aqueous Electrolytes for Lithium Ion Batteries: Method Development, Application and Lessons Learned, J. Electrochem. Soc. 162 (2015) A2500–A2508. https://doi.org/10.1149/2.0121514jes.

[23] E. Kramer, S. Passerini, M. Winter, Dependency of Aluminum Collector Corrosion in Lithium Ion Batteries on the Electrolyte Solvent, ECS Electrochem. Lett. 1 (2012) C9–C11. https://doi.org/10.1149/2.004205eel.

[24] S.H.N. Lim, D.R. McKenzie, M.M.M. Bilek, van der Pauw method for measuring resistivity of a plane sample with distant boundaries, Rev. Sci. Instrum. 80 (2009) 075109. https://doi.org/10.1063/1.3183503.

[25] M. Armandi, B. Bonelli, F. Geobaldo, E. Garrone, Nanoporous carbon materials obtained by sucrose carbonization in the presence of KOH, Microp. Mesop. Mater. 132 (2010) 414–420. https://doi.org/10.1016/j.micromeso.2010.03.021.

[26] M. Armandi, B. Bonelli, K. Cho, R. Ryoo, E. Garrone, Study of hydrogen physisorption on nanoporous carbon materials of different origin, Int. J. Hydrogen Energy 36 (2011) 7937–7943. https://doi.org/10.1016/j.ijhydene.2011.01.049.

[27] P.K.C.C.M. Conrad, Kinetics of the Pyrolysis of Cotton Cellulose, Text. Res. J. 36 (1966) 487–494.

[28] G. Várhegyi, M.J. Antal, E. Jakab, P. Szabó, Kinetic modeling of biomass pyrolysis, J. Anal. Appl. Pyrolysis. 42 (1997) 73–87. https://doi.org/10.1016/S0165-2370(96)00971-0.

[29] J. Scheirs, G. Camino, W. Tumiatti, Overview of water evolution during the thermal degradation of cellulose, Eur. Polym. J. 37 (2001) 933–942. https://doi.org/10.1016/S0014-3057(00)00211-1.

[30] R. Bacon, M.M. Tang, Carbonization of cellulose fibers - II. Physical property study, Carbon N. Y. 2 (1964) 221–225. https://doi.org/10.1016/0008-6223(64)90036-3.

[31] J.A. Lie, M.-B. Hägg, Carbon membranes from cellulose: Synthesis, performance and regeneration, J. Memb. Sci. 284 (2006) 79–86. https://doi.org/10.1016/j.memsci.2006.07.002.

[32] Y.P. Wu, E. Rahm, R. Holze, Carbon anode materials for lithium ion batteries, J. Power Sources 114 (2003) 228–236. https://doi.org/10.1016/S0378-7753(02)00596-7.

[33] Á.B. Palotás, L.C. Rainey, A.F. Sarofim, J.B. Vander Sande, P. Ciambelli, Effect of Oxidation on the Microstructure of Carbon Blacks, Energy & Fuels 10 (1996) 254–259. https://doi.org/10.1021/ef950168j.

[34] A. Khan, P. Jagdale, M. Castellino, M. Rovere, Q. Jehangir, P. Mandracci, C. Rosso, A. Tagliaferro, Innovative functionalized carbon fibers from waste: How to enhance polymer composites properties, Compos. Part B Eng. 139 (2018) 31–39. https://doi.org/10.1016/j.compositesb.2017.11.064.

[35] M. Bartoli, M. Giorcelli, C. Rosso, M. Rovere, P. Jagdale, A. Tagliaferro, Influence of Commercial Biochar Fillers on Brittleness/Ductility of Epoxy Resin Composites, Appl. Sci. 9 (2019) 3109. https://doi.org/10.3390/app9153109.

[36] K. Shirvanimoghaddam, B. Czech, A.E. Wiącek, W. Ćwikła-Bundyra, M. Naebe, Sustainable carbon microtube derived from cotton waste for environmental applications, Chem. Eng. J. 361 (2019) 1605–1616. https://doi.org/10.1016/j.cej.2018.11.157.

[37]   J. Xu, Y. Dou, Z. Wei, J. Ma, Y. Deng, Y. Li, H. Liu, S. Dou, Recent Progress in Graphite Intercalation Compounds for Rechargeable Metal (Li, Na, K, Al)-Ion Batteries, Adv. Sci. 4 (2017) 1700146. https://doi.org/10.1002/advs.201700146.

[38]   Y. Jiang, J. Liu, Definitions of Pseudocapacitive Materials: A Brief Review, En. Environ. Mater. 2 (2019) 30–37. https://doi.org/10.1002/eem2.12028.

[39]   N. Takami, A. Satoh, M. Oguchi, H. Sasaki, T. Ohsaki, ^{7}Li NMR and ESR analysis of lithium storage in a high-capacity perylene-based disordered carbon, J. Power Sources 68 (1997) 283–286. https://doi.org/10.1016/S0378-7753(97)02529-9.

[40]   J.R. Dahn, A.K. Sleigh, H. Shi, J.N. Reimers, Q. Zhong, B.M. Way, Dependence of the electrochemical intercalation of lithium in carbons on the crystal structure of the carbon, Electrochim. Acta. 38 (1993) 1179–1191. https://doi.org/10.1016/0013-4686(93)80048-5.

[41]   M. Winter, The Solid Electrolyte Interphase – The Most Important and the Least Understood Solid Electrolyte in Rechargeable Li Batteries, Zeitschrift Für Phys. Chemie. 223 (2009) 1395–1406. https://doi.org/10.1524/zpch.2009.6086.

[42]   F. Holtstiege, A. Wilken, M. Winter, T. Placke, Running out of lithium? A route to differentiate between capacity losses and active lithium losses in lithium-ion batteries, Phys. Chem. Chem. Phys. 19 (2017) 25905–25918. https://doi.org/10.1039/C7CP05405J.

[43]   E. Peled, The Electrochemical Behavior of Alkali and Alkaline Earth Metals in Nonaqueous Battery Systems - The Solid Electrolyte Interphase Model, J. Electrochem. Soc. 126 (1979) 2047. https://doi.org/10.1149/1.2128859.

[45]   C. Gerbaldi, All-solid-state lithium-based polymer cells for high-temperature applications, Ionics 16 (2010) 777–786. https://doi.org/10.1007/s11581-010-0484-4.

[45]   S. Yoon, J.H. Ryu, S.M. Oh, C. Lee, A preparation of carbon fibers using a block copolymer

surfactant template and its application to anode of lithium ion batteries, J. Non. Cryst. Solids. 355 (2009) 913–915. https://doi.org/10.1016/j.jnoncrysol.2009.04.010.

[46] S. Ahn, Y. Kim, K.J. Kim, T.H. Kim, H. Lee, M.H. Kim, Development of high capacity, high rate lithium ion batteries utilizing metal fiber conductive additives, J. Power Sources 81–82 (1999) 896–901. https://doi.org/10.1016/S0378-7753(99)00133-0.

[47] P. Meister, H. Jia, J. Li, R. Kloepsch, M. Winter, T. Placke, Best Practice: Performance and Cost Evaluation of Lithium Ion Battery Active Materials with Special Emphasis on Energy Efficiency, Chem. Mater. 28 (2016) 7203–7217. https://doi.org/10.1021/acs.chemmater.6b02895.

[48] Z. Le, W. Zhang, W. Li, J. Tan, R. Li, X. Wang, Y.V. Kaneti, X. Jiang, J. Chu, Y. Yamauchi, M. Hu, Metal-Organic Powder Thermochemical Solid-Vapor Architectonics toward Gradient Hybrid Monolith with Combined Structure-Function Features, Matter 3 (2020) 879–891. https://doi.org/10.1016/j.matt.2020.07.002.

[49] Y. Idemoto, J.W. Richardson, N. Koura, S. Kohara, C.-K. Loong, Crystal structure of $(Li_xK_{1-x})_2CO_3$ (x = 0, 0.43, 0.5, 0.62, 1) by neutron powder diffraction analysis, J. Phys. Chem. Solids. 59 (1998) 363–376. https://doi.org/10.1016/S0022-3697(97)00209-6.

[50] D.-T. Ngo, R. Scipioni, S.B. Simonsen, P.S. Jørgensen, S.H. Jensen, A TEM study of morphological and structural degradation phenomena in $LiFePO_4$-CB cathodes, Int. J. Energy Res. 40 (2016) 2022–2032. https://doi.org/10.1002/er.3575.

[51] S. Bhattacharya, A.R. Riahi, A.T. Alpas, Thermal cycling induced capacity enhancement of graphite anodes in lithium-ion cells, Carbon N. Y. 67 (2014) 592–606. https://doi.org/10.1016/j.carbon.2013.10.032.

[52] O.Y. Grigoreva, T.L. Kulova, S. V Pushko, A.M. Skundin, Lithium Intercalation into

Graphite during Direct Contact and Anodic Polarization, Russ. J. Electrochem. 38 (2002) 1327–1333. https://doi.org/10.1023/A:1021672822768.

[53] Y. Guo, R.B. Smith, Z. Yu, D.K. Efetov, J. Wang, P. Kim, M.Z. Bazant, L.E. Brus, Li Intercalation into Graphite: Direct Optical Imaging and Cahn-Hilliard Reaction Dynamics, J. Phys. Chem. Lett. 7 (2016) 2151–2156. https://doi.org/10.1021/acs.jpclett.6b00625.

[54] Y. Qian, C. Schultz, P. Niehoff, T. Schwieters, S. Nowak, F.M. Schappacher, M. Winter, Investigations on the electrochemical decomposition of the electrolyte additive vinylene carbonate in Li metal half cells and lithium ion full cells, J. Power Sources 332 (2016) 60–71. https://doi.org/10.1016/j.jpowsour.2016.09.100.

[55] M.R. Libera, R.F. Egerton, Advances in the Transmission Electron Microscopy of Polymers, Polym. Rev. 50 (2010) 321–339. https://doi.org/10.1080/15583724.2010.493256.

[56] L. Dupont, S. Laruelle, S. Grugeon, C. Dickinson, W. Zhou, J.-M. Tarascon, Mesoporous Cr_2O_3 as negative electrode in lithium batteries: TEM study of the texture effect on the polymeric layer formation, J. Power Sources 175 (2008) 502–509. https://doi.org/10.1016/j.jpowsour.2007.09.084.

[57] K. Amine, C.H. Chen, J. Liu, M. Hammond, A. Jansen, D. Dees, I. Bloom, D. Vissers, G. Henriksen, Factors responsible for impedance rise in high power lithium ion batteries. J Power Sources 97-98 (2001) 684-687. https://doi.org/10.1016/S0378-7753(01)00701-7

[58] H. Lu, J. Hagberg, G. Lindbergh, A. Cornell, Flexible and Lightweight Lithium-Ion Batteries Based on Cellulose Nanofibrils and Carbon Fibers, Batteries 4 (2018) 17. https://doi.org/10.3390/batteries4020017.

[59] Y. Li, Y.-S. Hu, M.-M. Titirici, L. Chen, X. Huang, Hard Carbon Microtubes Made from

Renewable Cotton as High-Performance Anode Material for Sodium-Ion Batteries, Adv. Energy Mater. 6 (2016) 1600659. https://doi.org/10.1002/aenm.201600659.

[60   H. Mao, L. Liu, L. Shi, H. Wu, J. Lang, K. Wang, T. Zhu, Y. Gao, Z. Sun, J. Zhao, G. Gao, D. Zhang, W. Yan, S. Ding, High loading cotton cellulose-based aerogel self-standing electrode for Li-S batteries, Sci. Bull. 65 (2020) 803–811. https://doi.org/10.1016/j.scib.2020.01.021.

[61]   Z. Gao, N. Song, Y. Zhang, X. Li, Cotton-Textile-Enabled, Flexible Lithium-Ion Batteries with Enhanced Capacity and Extended Lifespan, Nano Lett. 15 (2015) 8194–8203. https://doi.org/10.1021/acs.nanolett.5b03698.

[62]   L. Jabbour, M. Destro, D. Chaussy, C. Gerbaldi, S. Bodoardo, N. Penazzi, D. Beneventi, Cellulose/graphite/carbon fibres composite electrodes for Li-ion batteries, Compos. Sci. Technol. 87 (2013) 232–239. https://doi.org/10.1016/j.compscitech.2013.07.029.